The Effects of Increasing Lithium Deposition on the Power Exhaust Channel in NSTX

T.K. Gray[1], J.M. Canik[1], R. Maingi[1], A.G. McLean[2], J-W. Ahn[1], M.A. Jaworkski[3], R. Kaita[3], T.H. Osborne[4], S.F. Paul[3], F. Scotti[3], V.A. Soukhanovskii[2]

[1]Oak Ridge National Laboratory, Oak Ridge, TN. USA
[2]Lawrence Livermore National Laboratory, Livermore, CA. USA
[3]Princeton Plasma Physics Laboratory, Princeton, NJ. USA
[4]General Atomics, San Diego, CA. USA

E-mail contact of main author: tkgray@pppl.gov

Abstract. Previous measurements on the National Spherical Torus Experiment (NSTX) demonstrated peak, perpendicular heat fluxes, $q_{dep,\,pk} \leq 15$ MW/m^2 with an inter-ELM integral heat flux width, $\lambda_{q,\,int} \sim 3$—7 mm during high performance, high power operation (plasma current, $I_p = 1.2$ MA and injected neutral beam power, $P_{NBI} = 6$ MW) when magnetically mapped to the outer midplane. Analysis indicates that $\lambda_{q,\,int}$ scales approximately as I_p^{-1}. The extrapolation of the divertor heat flux and λ_q for NSTX-U are predicted to be upwards of 24 MW/m^2 and 3 mm respectively assuming a high magnetic flux expansion, $f_{exp} \sim 30$, $P_{NBI} = 10$ MW, balance double null operation and boronized wall conditioning. While the divertor heat flux has been shown to be mitigated through increased magnetic flux expansion, impurity gas puffing, and innovative divertor configurations on NSTX, the application of evaporative lithium coatings in NSTX has shown reduced peak heat flux from 5 to 2 MW/m^2 during similar operation with 150 and 300 mg of pre-discharge lithium evaporation respectively. Measurement of divertor surface temperatures in lithiated NSTX discharges is achieved with a unique dual-band IR thermography system to mitigate the variable surface emissivity introduced by evaporative lithium coatings. This results in a relative increase divertor radiation as measured by the divertor bolometry system. While the measure divertor heat flux is reduced with heavy lithium evaporation, λ_q contracts to 3—6 mm at low I_p but remains constant as I_p is increased to 1.2 MA yielding λ_q's comparable to no lithium discharges at high I_p.

1. Introduction

Spherical tokamaks (STs) have advantages over traditional aspect ratio tokamaks in that a potential DEMO fusion reactor or Fusion Nuclear Science Facility (FNSF) could be designed to operate at higher β and with a more compact size. However, due to their compact nature, the plasma facing components (PFCs) in divertors of STs can be subject to large heat and particle loads. These unmitigated heat fluxes will erode and possibly destroy the PFCs leading to machine downtime and eventual replacement of the divertor PFCs. Current cooling technologies, such as those implemented for ITER[1], limit the incident divertor heat flux to ≤ 10 MW/m^2. However, the upgraded National Spherical Torus Experiment (NSTX-U) planned for initial operation in 2014[2] is predicted to experience unmitigated heat fluxes up to 25 MW/m^2 operating in a double-null configuration with a large magnetic flux expansion, f_{exp}~30. Because of this, there is currently a major research thrust into mitigating the divertor heat flux for the ST as well as ITER. This could include some combination of a detached or radiative divertor, high f_{exp}[3,4,5], and/or a snowflake divertor[6,7].

Results from NSTX[8], EAST, smaller limiter tokamaks[9,10] and stellarators[11] have demonstrated the positive benefits of lithium wall conditioning techniques. These include increased energy confinement time[11,12], reduced power threshold to H-mode[13,14], reduced divertor recycling[15] and the elimination of Edge Localized Modes (ELMs)[16]. NSTX now routinely uses lithium as a wall conditioning technique instead of boronization[17]. The focus of this work will study the effect of varying amounts of pre-discharge lithium evaporation on

the power exhaust channel in NSTX. A discussion of NSTX experiment and diagnostics used follows in the next section. Section 3 will present results of varying lithium evaporation amounts on the peak divertor heat flux as well as the power scrape-off layer width, λ_q. Finally, section 4 will summarize the observed results.

2. Experimental Set-up

NSTX is a medium size spherical torus with a major radius, R_M=0.85 m and minor radius, $a_m \leq 0.65$ m ($A \geq 1.27$). Plasma current, I_p can be varied from 0.6–1.4 MA, with toroidal magnetic field, B_T in the range of 0.35-0.55 T and discharge lengths of ≤ 1.8 s. Plasma heating is achieved by neutral beam injection typically ranging in injected power $1 \leq P_{NBI} \leq 7.4$ MW with core electron temperatures, $T_e(0)$ = 0.6-1.5 keV and line-average electron densities, ne = 1–8(10)^{19} m^{-3}.

Since 2006 NSTX has employed evaporative lithium wall conditioning of its ATJ graphite plasma facing surfaces during some or all of the run campaign[17]. Lithium is evaporated onto the lower divertor prior to the discharge from 2 lithium ovens located on top of NSTX and toroidally displaced by 120° as shown in Fig. 1a. Typical pre-discharge lithium depositions can range from 10–300 mg though much larger depositions have been used. For boronized discharges, an Indigo Omega IR camera operated at a 30 Hz frame rate is used to measure surface temperature, which is derived from both an ex-*situ* calibration with a blackbody calibration source as well as an in-*situ* calibration during vacuum bake-outs that takes into account window transmission[18]. For lithiated discharges a fast Santa Barbra Focal Plane IR camera[19], equipped with dual-band optics to capture medium wavelength IR (MWIR: 7–10 μm) and long wavelength IR (LWIR: 10–13 μm) images on the camera simultaneously[20], is used to determine the divertor surface temperature independent of changes in surface emissivity due to the lithium evaporation. The dual-band IR camera was operated at 1.6 kHz and used the same calibration procedure as the Indigo Omega IR camera. Heat flux is then determined by a 2-D (radial and into the divertor tile) finite difference code THEODOR[21] using the measured divertor surface temperature, T_{surf} as the front face boundary condition. Data from the fast IR camera are then numerically averaged to an equivalent 30 Hz frame rate for comparison with the boronized data set.

Figure 2 shows a comparison between 2 NSTX discharges with 150 mg and 300 mg of lithium evaporation respectively. Both discharges are otherwise

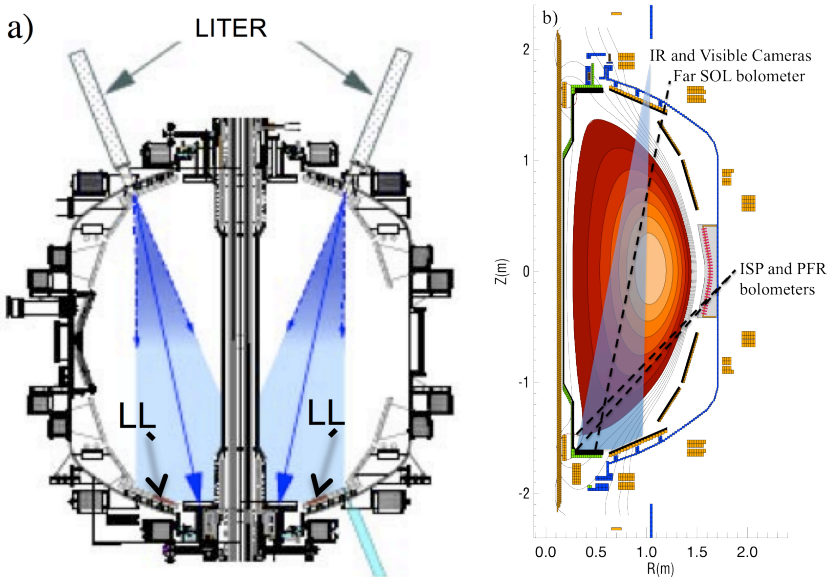

FIG.1. a) A schematic of the lithium evaporators in NSTX injecting lithium vapor to coat the lower divertor surfaces including LLD. b) Poloidal cross-section of a typical high δ NSTX discharge showing the diagnostics views.

similar with I_p=0.8 MA, P_{NBI} = 4 MW, though the 150 mg discharge had some initial pre-heating up to 5 MW from t = 0.1–0.25 s, and strong plasma shaping with high triangularity, δ ~0.7 and elongation, ~ 2.2. The 300 mg discharge also required higher gas puffing to fuel the discharge and avoid locked modes. Figures 2c and d show similar line averaged core densities and stored energies. The power crossing through the last closed flux surface, P_{SOL}, which is given by $P_{SOL} = P_{oh} + P_{NBI} - P_{core}^{rad} - W_p$, where P_{oh} is the ohmic heating power, P_{rad}^{core} is the core radiated power and W_p is the time rate of change of the plasma energy, is shown in Fig. 2c. Other than the initial pre-heating differences from 0.1–0.25 s, P_{SOL} is comparable between the 2 discharges.

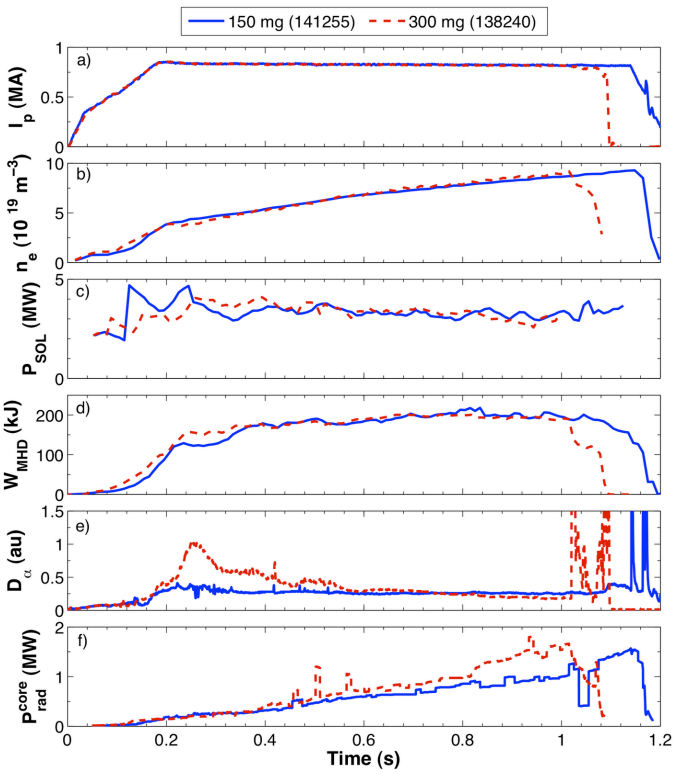

FIG.2. Comparison of a) Plasma current, I_p; b) line averaged density, n_e; c)power crossing the last-closed flux surface, P_{SOL}; d) Stored Energy, W_{MHD}; e) Divertor D_α emission; and f) Core Radiated Power, P_{rad}^{core} for 150 (–) and 300 mg (– –) 0.8 MA discharges and P_{NBI} = 4 MW.

3. Results

It has been previously reported that the addition of lithium to the divertor of NSTX had the effect of narrowing the heat flux width, λ_q[5]. Assuming P_{SOL} is similar for the 150 and 300 mg discharges, one would expect the peak heat flux to increase as λ_q contracts to conserve power. However, as shown in Fig. 3, the peak deposited heat flux, $q_{dep,\ pk}$ is actually reduced with sufficient lithium evaporation, in this case 300 mg is used, from 7 MW/m^2 to 2 MW/m^2. The result is a clear reduction in the power deposited by the plasma at the outer strike point. When only 150 mg of lithium evaporation is employed, the divertor heat flux at the outer strike point is similar to the boronized reference discharge. This indicates that there is a threshold amount of lithium influx into the divertor required to achieve a reduction in the deposited heat flux.

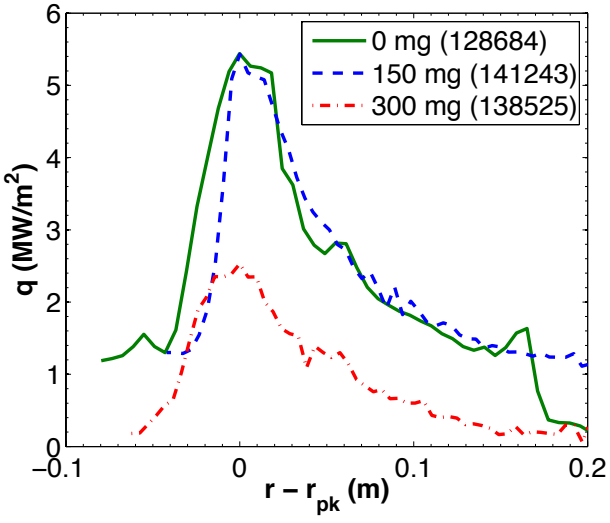

FIG.3. Radial heat flux profile for discharges with 0mg (boronized) (–), 150 mg (– –) and 300 mg (–.–) of lithium evaporation before the discharges.

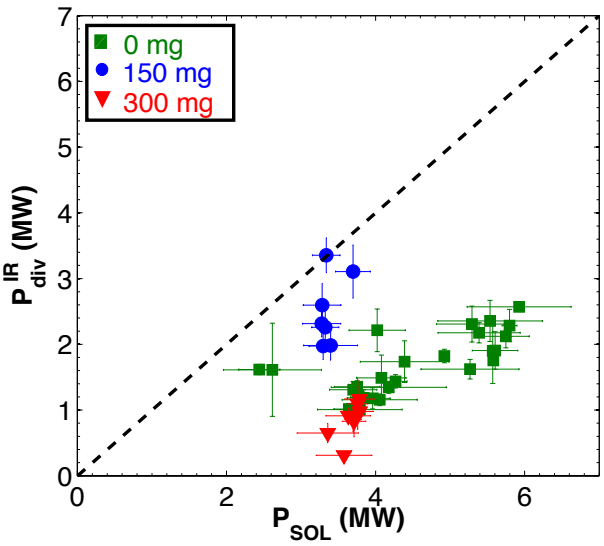

FIG.4. Incident divertor power measured at the outer strike point as a function of power crossing the last closed flux surface for 0, 150 and 300 mg of lithium deposition.

3.1. Heat Flux

The effects of increasing lithium deposition on power accounting at the outer strike point in divertor can be seen in Fig. 4. For 0 mg (boronized) discharges, power accounting as measured by the ration of P_{div}^{IR}/P_{SOL} ranges from 0.35 - 0.5. With the addition of 150 mg of lithium, divertor power accounting improves to 0.75 - 1. However, increasing the lithium deposition to 300 mg reduces P_{div}^{IR}/P_{SOL} to 0.125 - 0.2. Figure 5 shows time traces of I_p and the measured divertor surface temperature at the outer strike point, $T_{surf,\ OSP}$ and $q_{dep,\ pk}$ over the entire discharges shown in Fig. 2. A clear reduction in $T_{surf,\ OSP}$ is observed in Fig. 5b for these 0.8 MA shots that are otherwise nearly identical. There are differences in the gas puff rate used to fuel each discharge since a significant increase in fueling is required for the 300 mg discharge. Likewise, due to the increased lithium evaporation, the carbon content in the core plasma is higher and therefore P^{core}_{rad} is increased for the 300 mg discharge. However, from Fig. 2c, the difference in P_{SOL} is only significant during the initial NBI pre-heating from 0.1-0.25 s.

The reduction of $T_{surf,\ OSP}$ by 40–50% with increased pre-discharge lithium evaporation leads to a reduction in the computed heat flux. Figure 5c shows a reduction from $q_{dep,\ pk}$ = 5 MW/m^2 to ≤ 3 MW/m^2 at t=0.4 s. $q_{dep,\ pk}$ tends to decrease as the discharge progresses due to a secular density rise in the core plasma[5]. Because of this, comparison of the 2 discharges is typically limited to discharges times after the H-mode transition is

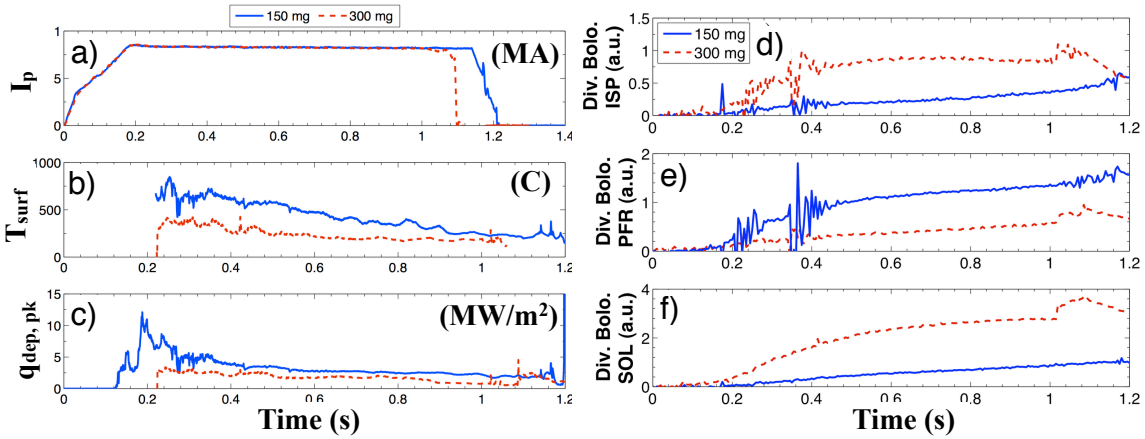

FIG.5. a) I_p (shown again for reference); b) divertor surface temperature at the outer strike point, $T_{surf,\ OSP}$; c) Peak deposited heat flux, $q_{dep,\ pk}$ and relative changes in divertor radiation measurements from 3 bolometry chords located at d) the Inner Strike Point (ISP), e) the Private Flux Region (PFR), f) the far Scrape-off Layer (SOL). for the lithium discharges shown previously in Fig. 1b.

achieved and before $q_{dep,\ pk}$ begins to decrease due to the secular density rise. $q_{dep,\ pk}$ for the 150 mg discharge only approaches $q_{dep,\ pk}$ for the 300 mg discharge around t=0.8 s. While only two discharges are being compared in Fig. 5, the trend remains intact for all I_p and P_{NBI} conditions observed to date. This can be seen in Fig. 6 where the 150 mg data shows $q_{\|,\ pk}$ linearly increasing with increasing I_p. The 300 mg data shows a similar linear trend with some overlap with the 150 mg dataset except $q_{\|,\ pk}$ is in general lower compared to the 150mg data. The 300mg data also appears to flatten for $I_p \geq 1.1$ MA though more data at higher I_p will be required to determine if the trend continues.

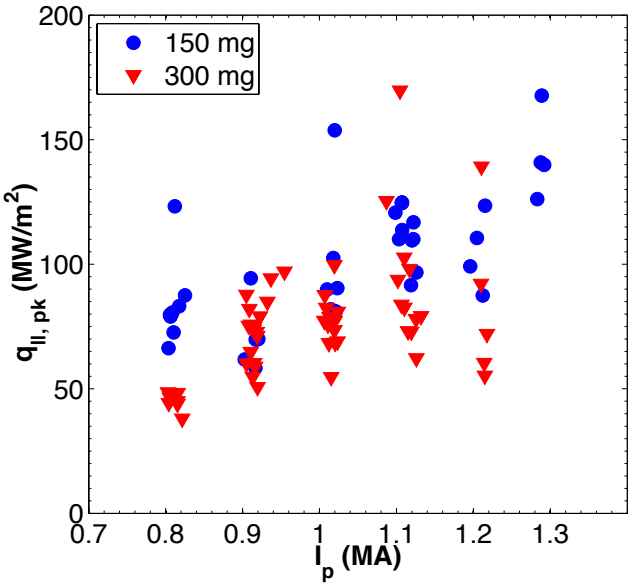

FIG.6. Peak parallel divertor heat flux, measured at the outer strike point versus I_p for 150 and 300mg of pre-discharge lithium evaporation for P_{NBI} = 4 MW and $\delta \sim 0.7$.

Figures 5d-f show the relative changes in divertor radiation as measured by divertor bolometry. The divertor bolometer sight lines, shown in Fig. 1b, look through the core plasma. From Fig. 2f, the magnitude of the core radiation is similar up to 0.6 s and don't diverge significantly until 0.8 s. Therefore, comparison of the divertor bolometer data from the 150 and 300 mg discharges is still possible since the contribution from the core plasma is similar between the two discharges. Figure 5d shows that divertor radiation at the inner strike point (ISP) is a factor of 4 higher in the 300 mg discharge than the 150 mg discharge early in the discharge ($t \leq 0.6$ s). Figure 5f shows similar trends at the OSP. Conversely, Fig. 5e shows the opposite trend in the Private Flux Region (PFR). Divertor radiation is increased for the lower lithium deposition amounts by also the same factor of 4. The reason for this is still under investigation, but could be due to the reduction in MARFE activity in the X-point region with lithium as has been shown previously[22].

Langmuir probe measurements are available from one probe located at r=0.495 m. The probe data are averaged from t = 0.4 ± 0.050 s. During this time, the probe is located in the near SOL of the 150 and 300 mg discharges (ψ_N = 1.04 and 1.06, respectively). From these measurements, shown in Table 1, there is an increase in divertor electron density from 4.3(10)^{19} to 7.4(10)^{19} m^{-3} an increase of 70%, while the electron temperature drops from 21 to 15 eV with increased lithium evaporation. Further, if the heat flux to the probe is estimated as, $q_{probe} \propto J_{sat}\ T_e^{3/2}$ and the sheath heat transmission factors are similar between the 150 and 300 mg discharges, than the relative decrease in the probe heat flux

Table.1. Divertor T_e and n_e determined from a divertor Langmuir probe located at r=0.495 m, in the far SOL at t=0.4 ± 0.050 s for the 150 and 300mg discharges shown in FIG.5.

	j_{sat} (A/m^2)	T_e (eV)	n_e (m^{-3})
150 mg (141255)	3.5(10)^3	21	4.3(10)^{19}
300 mg (138240)	3.9(10)^3	15	7.4(10)^{19}

is similar to the decrease in heat flux measured by the dual-band IR system.

3.2. Scrape-off Layer Width

Previous work has reported on the scaling of the power exhaust width, λ_q on NSTX with I_p and P_{SOL} for boronized wall conditions[5,23]. There it was found that the integral definition[24] of λ_q or $\lambda_{q,int}$ scales proportional with $I_p^{-1.6}$. Here we use the semi-empirical definition for λ_q that assumes the radial heat flux profile can be described by a diffusive gaussian[25] given by:

$$q(\bar{s}) = \frac{1}{2} q_0 \exp\left(\left(\frac{S}{2\lambda_q f_{exp}}\right)^2 - \frac{\bar{s}}{\lambda_q f_{exp}}\right) \mathrm{erfc}\left(\frac{S}{2\lambda_q f_{exp}} - \frac{\bar{s}}{S}\right) + q_{BG}, \qquad (1)$$

where s is the radial coordinate, s_0 the strike point location, $\bar{s} = s - s_0$, q_0 is the peak heat flux, q_{BG} is the background heat flux, λ_q is the e-folding length of the heat flux profile at midplane and S is the diffusive parameter and represents heat that has diffused into the PFR. For clarity, this λ_q is referred to as $\lambda_{q,\,Eich}$ to distinguish it from $\lambda_{q,\,int}$. Figure 7 shows how $\lambda_{q,\,Eich}$ and S vary as a function of I_p and lithium deposition amount. While there is scatter in the data, Fig. 6a shows that $\lambda_{q,\,Eich}$ contracts with I_p for all 3 lithium evaporation amounts of 0 mg (boronized), 150 and 300 mg. However, as additional lithium is introduced to the lower divertor of NSTX, $\lambda_{q,\,Eich}$ is decreased with respect to $\lambda_{q,\,Eich}$ values with no or less lithium as shown in Fig. 6a. However, at high I_p, $\lambda_{q,\,Eich}$ approaches similar values of ~ 2 mm. Figure 6b shows the diffusive parameter S as a function of I_p and for 0, 150 and 300 mg of lithium deposition. Here, S contracts with I_p for all three lithium depositions indicating that less energy is diffusing into the PFR as I_p is increased. However, the S values for 0 and 300 mg of lithium are comparable with $1 \lesssim S \lesssim 5$ mm. While the 150 mg dataset S values are on average lower $0.5 \lesssim S \lesssim 1.5$ mm. Again, at high I_p for all 3 lithium deposition amounts, S values of < 1 mm are common although there is significant scatter in the datasets.

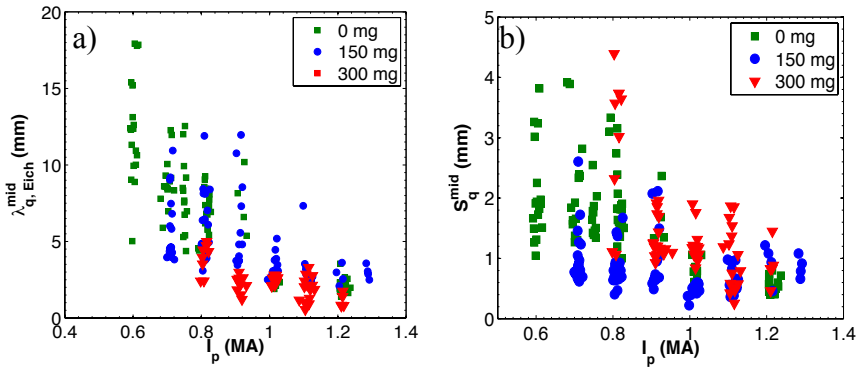

FIG.7. Inter-ELM averaged (30 Hz) a) $\lambda_{q,\,Eich}$ and b) S as a function of I_p for 0 mg (●), 150 mg (◆) and 300 mg (■) pre-discharge lithium evaporations where $\delta \sim 0.7$ and $P_{NBI} = 4$ MW.

3.3. Progressively Increased Lithium Deposition

Heat flux data, taken during the 2008 run campaign and discussed in the literature[15,16,26], show trends in $\lambda_{q,\,Eich}$ and S as pre-discharge lithium evaporation is progressively increased. These discharges are lower δ (~ 0.5) with P_{NBI} = 2-4 MW. Lower beam power was required as the lithium deposition was increased due to global stability limits being reached and leading to disruptions. This dataset also pre-dates the dual-band IR camera system on NSTX and as such the magnitude of the heat flux is questionable, but previous observations[5] show that the overall shape of the heat flux profile is consistent between single and dual-band IR measurements. The heat flux data for t = 0.25-0.45 were non-linearly fit to Eq. 1 for each discharge and then averaged over a time window of 0.25 -

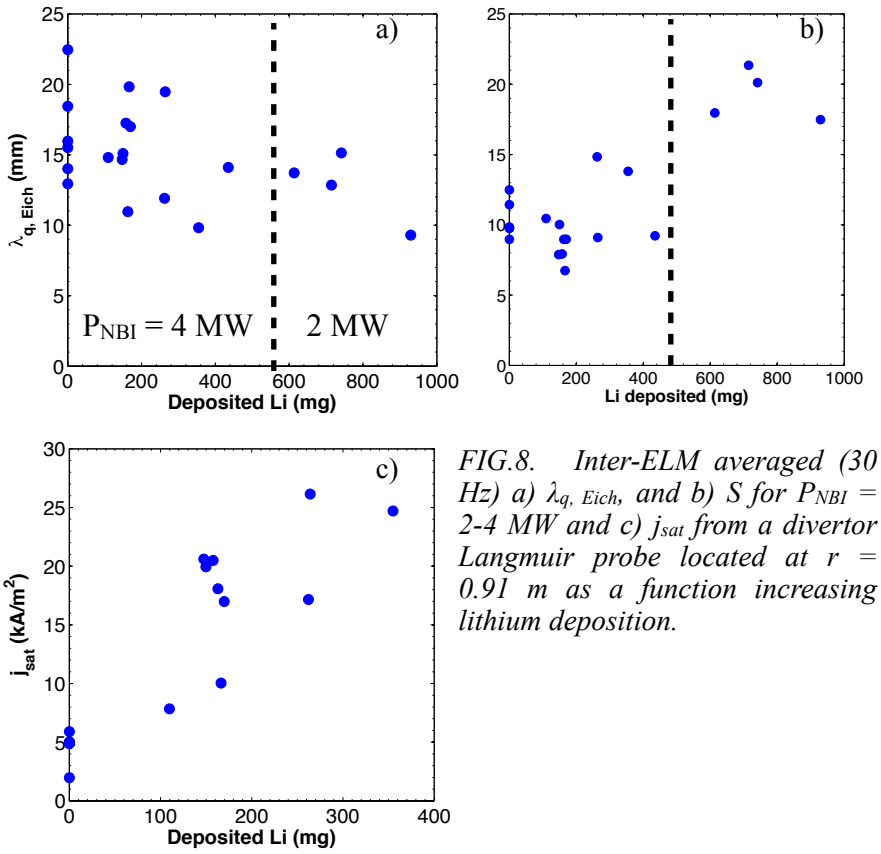

FIG.8. Inter-ELM averaged (30 Hz) a) $\lambda_{q,\,Eich}$, and b) S for P_{NBI} = 2-4 MW and c) j_{sat} from a divertor Langmuir probe located at r = 0.91 m as a function increasing lithium deposition.

0.45 s which was chosen to ensure data were during the H-mode but prior to the density roll-over typically seen in NSTX heat flux data[5]. Fig. 8a shows that $\lambda_{q,\,Eich}$ decreases with the addition of more lithium. Since these data are inter-ELM averaged at 30 Hz, some of this decrease is due to suppression of small Type V ELMs which can be ubiquitous in NSTX discharges. However heat flux profiles that were integrated over type I ELMs were neglected from the average. However, the decrease in $\lambda_{q,\,Eich}$ continues after ELMs have been fully suppressed. The continued decrease in $\lambda_{q,\,Eich}$ could be due to continued pedestal modification[24] by increasing lithium deposition.

The diffusive parameter S, as seen in Fig. 8b, is unaffected or decreases slightly between 0 and 200 mg of lithium and then increases with further increases in lithium deposition. This is in general agreement with the high δ discharges in Fig. 7b which show a contraction in S from 0 to 150 mg of lithium but an increase when lithium is increased to 300 mg. The increase in lithium deposition appears to be correlated with increased diffusion of the heat flux into the PFR. This is due to the increase in divertor particle flux that results with increased lithium deposition as shown in Fig. 8c. The data in Fig. 8c is limited to < 400 mg of lithium because PNBI was reduced to 2 MW due to avoid global MHD modes.

4. Conclusions

Here we present heat flux data obtained on NSTX with varying amounts of pre-discharge lithium evaporation. Heat flux was determined by measuring the surface temperature of the divertor with a dual-band IR camera to reduce the effect of variable surface emissivity introduced by the lithium coatings. These measurements show not only a contraction in the heat flux footprint, but also a reduction in the heat flux when a threshold amount of lithium is used. The reduction in heat flux, even with a significantly contracted λ_q, shows an increase in divertor power accounting, as measured by the ratio of P_{div}^{IR}/P_{SOL}, with 150 mg when compared to boronized (0 mg) discharges. However, when the lithium deposition is increased to 300 mg, power accounting drops to between 12.5 - 20% of P_{SOL}. The decrease in divertor heat flux is accompanied by an increase in radiation at the inner strike point as

well as in the far SOL. However, radiation measured from the PFR is reduced with higher lithium deposition amounts. The reason for this variation is not well understood and interpretive modeling is planned to help address this issue. The contraction in the heat flux footprint, $\lambda_{q,\ Eich}$ appears to be proportional to both I_p and the amount of lithium deposited with the difference in $\lambda_{q,\ Eich}$ largely undistinguishable at high Ip where $\lambda_{q,\ Eich} \sim$ 1-2 mm regardless of the amount of lithium deposition. Additionally, the diffusive parameter S increases with lithium deposition above 200 mg but decreasing between 0 - 200 mg of lithium. The initial decrease in S is believed to be due to the reduced divertor recycling; while the increase in S above 200 mg is linked to the increased divertor particle flux with increased lithium deposition. The increased divertor flux increases the divertor collisionality and leads to increased diffusion of heat flux into the PFR and increased divertor radiation. The use of lithium to moderate divertor heat fluxes requires a threshold amount of lithium to achieve this. For high δ, high performance NSTX discharges, between 100 - 200 mg of lithium appears to be required for reduction in the heat flux to the divertor.

Acknowledgements
Work supported by U.S. Department of Energy contracts: DE-AC05-00OR22725, DE-AC52-07NA27344 and DE-AC02-09CH11466. The authors would also like to acknowledge a collaboration with A. Herrmann of IPP-Garching for the use of the THEODOR code.

References
[1] A. Loarte et. al., Nucl. Fusion **47** (2007) S203
[2] J.E. Menard, et al. Proceedings of the 37th EPS Conference on Plasma Phys. (2010)
[3] V.A. Soukhanovskii, et al. Nucl. Fusion **49** (2009) 095025
[4] V.A. Soukhanovskii, et al. Phys. Plasmas **16** (2009) 022501
[5] T.K. Gray, et al., J. Nucl. Mater. **415** (2011) S360-S364
[6] D.D. Ryutov. Phys. Plasmas **14** (2007) 064502
[7] V.A. Soukhanovskii, et al. J. Nucl. Mater. **415** (2011) S365–368
[8] M.A. Jaworski, et al., these proceedings. (2012)
[9] G. Mazzitelli, et. al., Nucl. Fusion **51** (2011) 073006
[10] S. Mirnov. J. Nucl. Mater. **390–391** (2009) 876885
[11] J. Sanchez, et. al., Nucl. Fusion **51** (2011) 094022
[12] M.G. Bell, et. al., Plasma Phys. Control. Fusion **51** (2009) 124054
[13] S.M. Kaye. et. al., Nucl. Fusion. **51** (2011) 113019
[14] H.Y. Guo, et. al., J. Nucl. Mater. **S415**(1) (2011) S369-S374
[15] R. Maingi, et. al., Phys. Rev. Lett. **105** (2011) 145004
[16] R. Maingi, et. al., Phys. Rev. Lett. **103** (2009) 075001
[17] H.W. Kugel, et. al. Phys. Plasmas **15** (2008) 056118
[18] D.M. Mastrovito, et al. Rev. Sci. Instrum. **74**(12) (2003) 50905092
[19] J-W. Ahn, et. al., Rev. Sci. Instrum. **81** (2010) 023501
[20] A.G. McLean, et al., Rev. Sci. Instrum. **83** (2012) ???
[21] A. Herrmann, proceeding of the 28th EPS conference on controlled Fusion and plasma physics, Madeira, 2001
[22] F. Scotti, et al., J. Nucl. Mater. **S415** (2011) S405-408
[23] R. Maingi, et. al. J. Nucl. Mater. **363–36**5 (2007) 196–200
[24] A. Loarte et al., J. Nucl. Mater. **266–269** (1999) 587–592.
[25] T. Eich,et. al., Phys. Rev. Lett. **107** (2011) 215001
[26] D. Boyle, et al., submitted to J. Nucl. Mater. (2012)